

MECHANISM STUDY ON OXYGEN VACANCY INDUCED RESISTANCE SWITCHING IN Au/LaMnO₃/SrNb_{0.01}Ti_{0.99}O₃

YU-LING JIN, ZHONG-TANG XU, KUI-JUAN JIN*, CHEN GE,
HUI-BIN LU and GUO-ZHEN YANG

*Beijing National Laboratory for Condensed Matter Physics,
Institute of Physics, Chinese Academy of Sciences, Beijing 100190, China*

**kjjin@iphy.ac.cn*

Received 21 January 2013

Revised 19 February 2013

Accepted 20 February 2013

Published 2 April 2013

Mechanism of resistance switching in heterostructure Au/LaMnO₃/SrNb_{0.01}Ti_{0.99}O₃ was investigated. In Au/LaMnO₃/SrNb_{0.01}Ti_{0.99}O₃ devices the LaMnO₃ films were fabricated under various oxygen pressures. The content of the oxygen vacancies has a significant impact on the resistance switching performance. We propose that the resistance switching characteristics of Au/LaMnO₃/SrNb_{0.01}Ti_{0.99}O₃ arise from the modulation of the Au/LaMnO₃ Schottky barrier due to the change of the oxygen vacancy concentration at Au/LaMnO₃ interface under the external electric field. The effect of the oxygen vacancy concentration on the resistance switching is explained based on the self-consistent calculation. Both the experimental and numerical results confirm the important role of the oxygen vacancies in the resistance switching behavior.

Keywords: Perovskite oxide; oxygen vacancy; resistive switching; self-consistent calculations.

PACS Number(s): 73.40.Ns, 77.80.Fm, 72.10.Bg

1. Introduction

Resistance switching effects have attracted considerable attention due to its potential applications in next generation nonvolatile memories with high density, great scalability and low power consumption.^{1,2} Up to now, resistance switching effects have been observed in a wide variety of perovskite oxides, such as manganites, titanates and zirconates, with metal-insulator-metal capacitor-like structures.³⁻⁶ The mechanisms of the resistance switching effects, however, remain elusive. To understand the underlying switching mechanisms, several theoretical models have been proposed, such as the modulation of the Schottky barrier,^{6,7} charge trapping and discharging,⁸⁻¹⁰ electrochemical migration of oxygen vacancies¹¹⁻¹⁵ and oxidation/reduction reaction.^{16,17}

In this paper, we investigate the role of the oxygen vacancies in the resistance switching performance and the effects of the concentration of the oxygen vacancies on the characteristics of resistance switching in Au/LMO/SNTO devices with LMO films fabricated under various oxygen pressures. Many works have investigated the correlation between the resistance switching properties and oxygen vacancies by controlling the concentration and the migration of oxygen vacancies via various techniques.^{18–23} The migration of oxygen vacancies (or oxygen ions) under an applied electric field, which has attracted great attentions, is considered to play an important role in these effects. Recently, we have shown that the amount of oxygen vacancies in LMO varies with the fabrication oxygen pressure using Aberration-Corrected Scanning Transmission Electron Microscopy (STEM) in Pt/LaMnO₃/SrNb_{0.01}Ti_{0.99}O₃ (SNTO) devices which exhibit varying degrees of hysteretic behaviors.²¹ The oxygen vacancy concentration in the LMO film has a significant impact on the resistance switching characteristics. The focus of this paper is on the correlation between the concentration of oxygen vacancy and the properties of Au/LMO Schottky junction. Because oxygen vacancies behave as mobile donors in LMO, their concentration can affect the carrier density. On the other hand, oxygen vacancies also act as impurities which have impact on the mobility of carriers. Our detailed analysis of the role played by the oxygen vacancies on the properties of Au/LMO Schottky junctions is presented based on the numerical calculation.

2. Experimental Techniques

Oxygen-deficient LMO films with a thickness of 100 nm were directly deposited on the SNTO substrates of the size $3 \times 5 \text{ mm}^2$ by computer-controlled laser molecular-beam epitaxy (LMBE), with a pulsed XeCl excimer laser beam ($\sim 20 \text{ ns}$, 2 Hz , $\sim 1.5 \text{ Jcm}^{-2}$, 308 nm) focused on a sintered ceramic LMO target. The SNTO substrates were carefully cleaned with alcohol, acetone and deionized water before being placed into the growth chamber. Subsequently, LMO films with a thickness of 100 nm were deposited at a temperature of 750°C under the oxygen pressures of 5×10^{-4} , 5×10^{-3} , 5×10^{-2} and 10 Pa , respectively, and *in situ* annealed under the same conditions for 20 min, before cooling down to room temperature in oxygen atmosphere. Gold was deposited on LMO/SNTO by pulsed laser deposition (PLD) as the top electrodes. The current–voltage (I – V) behaviors were measured by a Keithley 2400 source meter at room temperature. The forward-bias is defined by the positive voltage applied on the Au electrode. The experimental I – V curves were measured following the sequence of sweeping the voltage as $-1.5 \text{ V} \rightarrow 0 \text{ V} \rightarrow 3 \text{ V} \rightarrow 0 \text{ V} \rightarrow -1.5 \text{ V}$, which is depicted by four branches with arrows as shown in Fig. 1. In order to avoid the dielectric breakdown the maximum of negative-bias is only 1.5V. Thus, the resistance switching behavior is not very noticeable when under the reverse-bias. All data are quite stable in the present samples, and can be repeated after several months.

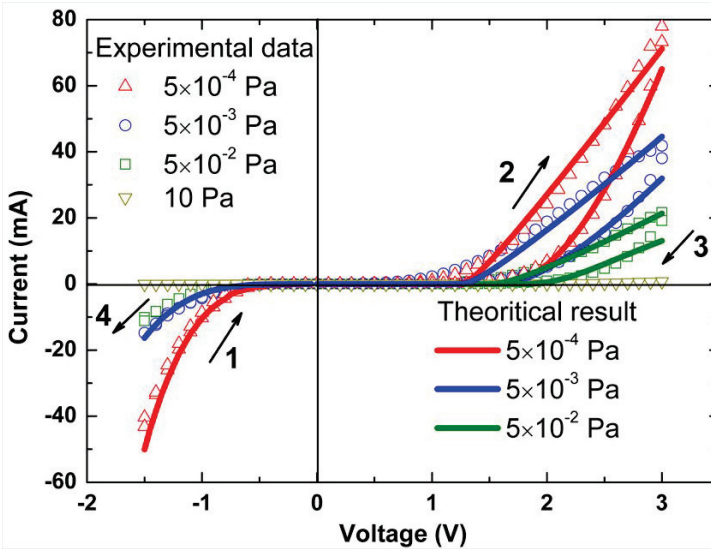


Fig. 1. (Color online) Measured and calculated I - V characteristics of Au/LMO/SNTO with LMO films fabricated under the oxygen pressures of 5×10^{-4} , 5×10^{-3} , 5×10^{-2} and 10 Pa. The forward-bias is defined by the positive voltage applied on the Au electrode. Arrows indicate the direction of bias sweeping.

3. Calculation Method

Figure 1 shows I - V characteristics both measured and calculated for the devices with the LMO films fabricated under various oxygen pressures. The resistance switching behavior happens under the forward-bias and is suppressed by increasing the fabrication oxygen pressure. It is well known that LMO is a typical perovskite oxide material as Mott insulator, and the properties of LMO films are affected by the chemical composition and oxygen content.^{24,25} Because the oxygen vacancies act as mobile donors with positive charges, the LMO films deposited on SNTO substrates under 5×10^{-4} , 5×10^{-3} , and 5×10^{-2} Pa oxygen pressure are all considered as n -type semiconductors. As the values of the work function of Au and SNTO are about 5.1²⁶ and 4.05 eV,²⁷ respectively, a Schottky barrier must be formed at the interface between Au and LMO, while the ohmic contact would appear at the interface between LMO and SNTO. Thus, the I - V loops exhibit obvious rectifying characteristics that are attributed to the Schottky junction formed at Au and LMO interface.

The properties of the Schottky junction formed at the Au and LMO interface can be obtained by self-consistently solving the Poisson and continuity equations.²⁸ The coupled equations with three primary variables: the electrostatic potential $\psi(x)$, the quasi-Fermi potential of electrons $\phi_n(x)$ and holes $\phi_p(x)$ are as follows:

$$\frac{\partial^2 \psi(x)}{\partial x^2} = -\frac{q}{\epsilon} (p(x) - n(x) + N_d), \quad (1)$$

$$\frac{\partial n(x)}{\partial t} = \frac{1}{q} \frac{\partial J_n(x)}{\partial x} - U(x), \quad (2)$$

$$\frac{\partial p(x)}{\partial t} = -\frac{1}{q} \frac{\partial J_p(x)}{\partial x} - U(x), \quad (3)$$

$$n(x) = n_i \exp\left(\frac{q}{kT}(\psi(x) - \phi_n(x))\right), \quad (4)$$

$$p(x) = n_i \exp\left(\frac{q}{kT}(\phi_p(x) - \psi(x))\right), \quad (5)$$

where $n(x)$ and $p(x)$ are the concentration of electrons and holes, respectively. $J_n(x)$ and $J_p(x)$ are the current density of electrons and holes, respectively. $U(x)$ is the recombination rate of the Shockley–Read–Hall recombination process.^{29–32} q , ε , N_d and n_i denote the electron charge, dielectric constant, ionized donor density and intrinsic carrier concentration, respectively. k and T denote the Boltzmann constant and temperature, respectively. Richardson thermionic current based on the thermionic-emission-diffusion theory²⁸ is employed as the current boundary condition.

$$J_n(x=0) = qv_n(n_s - n_0), \quad (6)$$

$$J_p(x=0) = -qv_p(p_s - p_0), \quad (7)$$

where v_n , v_p are the thermal velocities of the electrons and holes in the semiconductor respectively. n_s and p_s are the concentrations of the electrons and holes at the semiconductor surface respectively. n_0 and p_0 denote the concentrations of the electrons and holes under quasi-equilibrium condition respectively. Moreover, electrons in the metal are able to tunnel into the conduction band of LMO under the reverse-bias, so the tunneling current is included in our calculation. The tunneling current density of electrons is expressed as

$$j(x) = \frac{i\hbar}{2m_n^*} \left[\varphi(x) \frac{d\bar{\varphi}(x)}{dx} - \bar{\varphi}(x) \frac{d\varphi(x)}{dx} \right], \quad (8)$$

where $\varphi(x)$ is the wave function obtained by solving the one-dimensional single-particle Schrödinger equation using Numerov's method. The details of solving these equations were reported in Ref. 21.

4. Results and Discussion

The dramatic change in the resistance of Au/LMO/SNTO devices under the forward-bias is considered arising from modulating the Au/LMO Schottky barrier by the movement of oxygen vacancies. Because oxygen vacancies are positively charged, they can be repelled away from the interface of Au and LMO, when the positive bias is applied on the Au. Thus the height and width of Au/LMO Schottky barrier become higher and wider due to the decrease of the concentration of

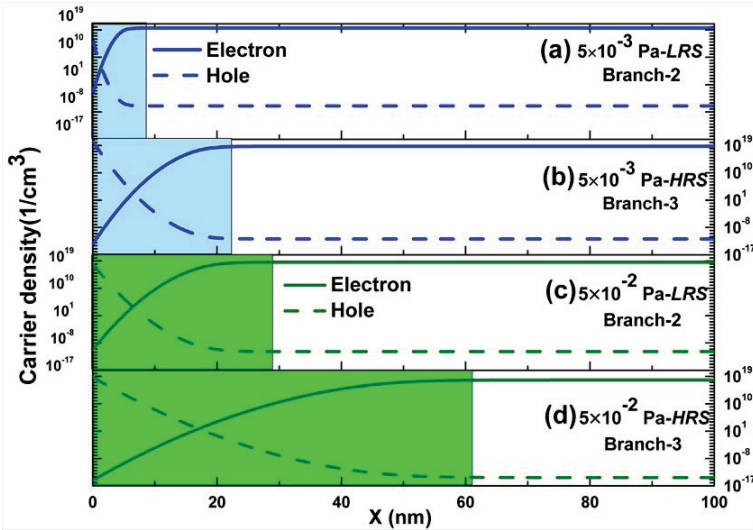


Fig. 2. (Color online) Carrier distribution by calculating in the LMO films fabricated under 5×10^{-3} and 5×10^{-2} Pa at LRS and HRS. The depletion layer is marked as a shaded area.

the oxygen vacancies. The possible influence of electrical Joule heating effect in this device cannot be avoided. The heating effect can influence the movement of the carriers and oxygen vacancies (oxygen ions), which may have impact on the unipolar switching behavior. However, the Joule heating is not the dominant mechanism in our devices with bipolar switching phenomenon.^{3,33} To minimize the heating effect, we stopped for two minutes after each point measuring.

We assume that the concentration of electrons in the vicinity of the Au/LMO interface decreases with decreasing the concentration of the oxygen vacancies, as the oxygen vacancies act as the donors in the oxides. The distribution of the electrons and holes of LMO films fabricated under 5×10^{-3} and 5×10^{-2} Pa at low resistance state (LRS) and high resistance state (HRS) are plotted in Fig. 2. The decreasing of the concentration of the electron results in the increase of the width of the depletion layer. Thus, the resistance of the Schottky junction, which contributes the major part of the whole resistance of the device, increases accordingly. As a result the resistance of the device is eventually switched from LRS to HRS with sufficient forward-bias.

The various contents of oxygen vacancies generated by the process of fabrication seem to be responsible for the varying resistance switching performances. Figure 1 shows the LMO film fabricated under 5×10^{-4} Pa exhibits the most pronounced resistance switching performance, while the resistance of the LMO film fabricated under 10 Pa is nearly unchanged in the external electric field. The I - V results in Fig. 1 show that the resistance of the device becomes smaller with more oxygen vacancies in the LMO film fabricated under lower oxygen pressure. The distributions of the carriers in Fig. 2 show that the LMO film fabricated under 5×10^{-3} Pa

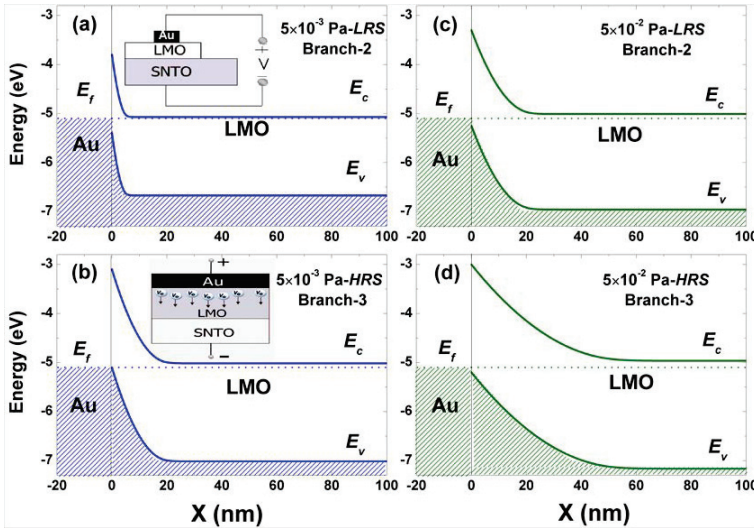


Fig. 3. (Color online) Calculated energy band diagrams of Au/LMO Schottky junctions at LRS and HRS, in which LMO film was fabricated under 5×10^{-3} and 5×10^{-2} Pa. The inset in (a) shows the measurement configuration of the devices. And the inset in (b) shows the schematic illustration of the movement of oxygen vacancies when the devices are under the forward-bias.

with more oxygen vacancies has more conducting electron. But the existence of the oxygen vacancies, which also act as impurities in LMO thin films, can affect the properties of LMO film simply by two ways of narrowing down the band gap for the impurity levels (quasi-continuous) lying in the band gap and reducing the carrier mobility for the impurities scattering. This assumption is reasonable, as some early studies on the *p*-doped lanthanum manganites have revealed that oxygen vacancies could decrease the band gap,³⁴ carrier (hole) density and mobility.^{35,36} The energy band structures obtained from the calculation of the Au/LMO Schottky junction at the LRS and HRS, in which LMO film was fabricated under 5×10^{-3} Pa, are plotted in Figs. 3(a) and 3(b), respectively. Figures 3(c) and 3(d) show the energy band structures with higher Schottky barriers of LMO film fabricated under 5×10^{-2} Pa at the LRS and HRS than that of LMO film fabricated under 5×10^{-3} Pa.

It is shown in Fig. 4 that higher electric field exists in the Au/LMO interface of the LMO film fabricated under 5×10^{-3} Pa compared with that fabricated under 5×10^{-2} Pa. The resistance switching behavior, which is assumed to originate from the movement of oxygen vacancies in the vicinity of Au/LMO Schottky junction as mentioned above, is enhanced by increasing of the oxygen vacancy density. The inset in (b) shows the schematic illustration of the movement of oxygen vacancies under the forward-bias. Because the oxygen vacancies are more free to move in the high electric field and the modulation effect on Au/LMO Schottky junction is more prominent as we can see from the profile of the energy band structure and the electric field. So more oxygen vacancies in LMO thin films result in larger variation

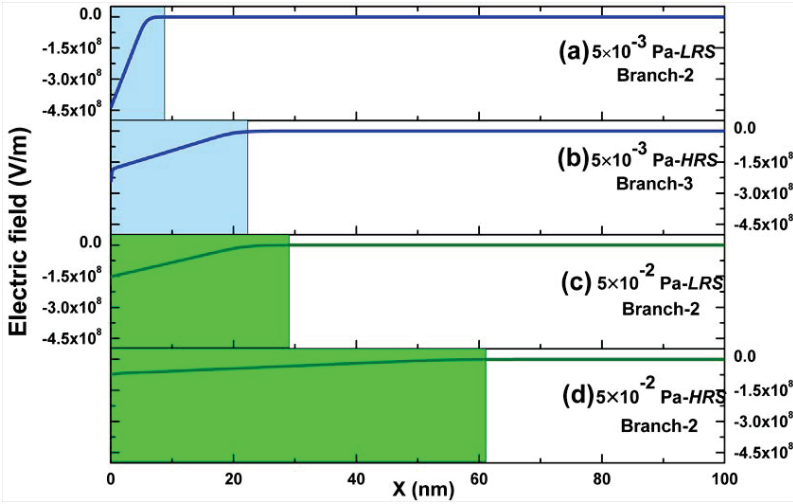


Fig. 4. (Color online) Calculated profiles of electric field in LMO films fabricated under 5×10^{-3} and 5×10^{-2} Pa at LRS and HRS. The depletion layer is marked as a shaded area.

of the Schottky barrier at Au and LMO interface. In addition, it is worth mentioned that the resistance switching performance of the LMO film grown under 5×10^{-4} Pa does not improve more than that of the LMO film grown under 5×10^{-3} Pa. This may be due to the excessive structural distortion caused by oxygen vacancies.

The series of parameters for calculating the process of resistance switching of the LMO films grown under various oxygen pressures are listed in Tables 1–3. The carrier concentration and mobility of LMO film fabricated under 5×10^{-3} Pa are $\sim 4 \times 10^{19} \text{ cm}^{-3}$ and $\sim 2 \text{ cm}^2 \text{ V}^{-1} \text{ s}^{-1}$, respectively, which were obtained by our measurements using a Quantum Design physical property measurement device (PPMS-9). The band gap of the LMO is taken from 1.5 eV to 2.0 eV, and the carrier mobility of manganese oxide is around $10 \text{ cm}^2 \text{ V}^{-1} \text{ s}^{-1}$, which is identical with the reported parameters in previous works.^{37–43} Our calculated results of the transport property and the switchable resistance effects, which are plotted in Fig. 1, have good agreements with the experimental data.

5. Conclusion

We have explained the role of the oxygen vacancy in the resistance switching effect by assuming they behave as mobile donors and impurities. Based on the drift-diffusion model, the change of the oxygen vacancy concentration at the Au/LMO Schottky interface under the external electric field is considered to be responsible for the resistance switching behaviors. The concentration of oxygen vacancies has a critical impact on the carrier density, band gap and carrier mobility of the LMO films and further affects the resistance switching characteristics of Au/LMO/SNTO devices. Compared with the experimental results, it indicated that the simulation

Table 1. Parameters used in calculation of the branch-1 of the process of resistance switching.

Fabrication oxygen pressure (Pa)	5×10^{-4}	5×10^{-3}	5×10^{-2}
Concentration (cm^{-3})	14×10^{19}	9.8×10^{19}	9.8×10^{19}
Mobility ($\text{cm}^2 \text{V}^{-1} \text{s}^{-1}$)	1.3	1.5	1.5
Band gap (eV)	1.53 ^b	1.55 ^b	1.55 ^b

Table 2. Parameters used in calculation of the branch-2 of the process of resistance switching.

Fabrication oxygen pressure (Pa)	5×10^{-4}	5×10^{-3}	5×10^{-2}
Concentration (cm^{-3})	8.5×10^{19}	$4.2 \times 10^{19\text{a}}$	3.8×10^{18}
Mobility ($\text{cm}^2 \text{V}^{-1} \text{s}^{-1}$)	1.8	2 ^a	13 ^c
Band gap (eV)	1.58 ^b	1.6 ^b	1.95 ^b

Table 3. Parameters used in calculation of the branch-3 of the process of resistance switching.

Fabrication oxygen pressure (Pa)	5×10^{-4}	5×10^{-3}	5×10^{-2}
Concentration (cm^{-3})	8.0×10^{18}	5×10^{18}	0.7×10^{18}
Mobility ($\text{cm}^2 \text{V}^{-1} \text{s}^{-1}$)	6	12 ^c	16 ^c
Band gap (eV)	1.9 ^b	2.0 ^b	2.2

^aParameters taken from Ref. 21.^bParameters taken from Refs. 37 and 41.^cParameters taken from Refs. 42–43.

results were reasonable and applicable, and this result would be helpful for understanding the underlying mechanism of the resistance switching.

Acknowledgments

This work was supported by the National Basic Research Program of China (Nos. 2012CB921403 and 2013CB328706) and the National Natural Science Foundation of China (Nos. 10825418 and 11134012).

References

1. R. Waser and M. Aono, *Nat. Mater.* **6** (2007) 833.
2. G. I. Meijer, *Science* **319** (2008) 1625.
3. A. Asamitsu, Y. Tomioka, H. Kuwahara and Y. Tokura, *Nature* **388** (1997) 50.
4. E. Lee, M. Gwon, D. W. Kim and H. Kim, *Appl. Phys. Lett.* **98** (2011) 132905.

5. M. H. Lin, M. C. Wu, Y. H. Huang, C. H. Lin and T. Y. Tseng, *IEEE Trans. Electron Devices* **58** (2011) 1182.
6. A. Sawa, *Mater. Today* **11** (2008) 28.
7. D. S. Jeong, H. Schroeder and R. Waser, *Phys. Rev. B* **79** (2009) 195317.
8. T. Harada, I. Ohkubo, K. Tsubouchi, H. Kumigashira, T. Ohnishi, M. Lippmaa, Y. Matsumoto, H. Koinuma and M. Oshima, *Appl. Phys. Lett.* **92** (2008) 222113.
9. Y. Xia, W. He, L. Chen, X. Meng and Z. Liu, *Appl. Phys. Lett.* **90** (2007) 022907.
10. D. Shang, Q. Wang, L. Chen, R. Dong, X. Li and W. Zhang, *Phys. Rev. B* **73** (2006) 245427.
11. Y. Nian, J. Strozier, N. Wu, X. Chen and A. Ignatiev, *Phys. Rev. Lett.* **98** (2007).
12. R. Waser, R. Dittmann, G. Staikov and K. Szot, *Adv. Mater.* **21** (2009) 2632.
13. T. Fujii, M. Kawasaki, A. Sawa, Y. Kawazoe, H. Akoh and Y. Tokura, *Phys. Rev. B* **75** (2007) 165101.
14. M. J. Rozenberg, M. J. Sánchez, R. Weht, C. Acha, F. Gomez-Marlasca and P. Levy, *Phys. Rev. B* **81** (2010) 115101.
15. M. Quintero, P. Levy, A. Leyva and M. Rozenberg, *Phys. Rev. Lett.* **98** (2007) 146403.
16. S. Tsui, A. Baikalov, J. Cmaidalka, Y. Y. Sun, Y. Q. Wang, Y. Y. Xue, C. W. Chu, L. Chen and A. J. Jacobson, *Appl. Phys. Lett.* **85** (2004) 317.
17. K. Tsubouchi, I. Ohkubo, H. Kumigashira, M. Oshima, Y. Matsumoto, K. Itaka, T. Ohnishi, M. Lippmaa and H. Koinuma, *Adv. Mater.* **19** (2007) 1711.
18. K. Shibuya, R. Dittmann, S. Mi and R. Waser, *Adv. Mater.* **22** (2010) 411.
19. S. Y. Wang, D. Y. Lee, T. Y. Huang, J. W. Wu and T. Y. Tseng, *Nanotechnology* **21** (2010) 495201.
20. L. Goux, P. Czarnecki, Y. Y. Chen, L. Pantisano, X. P. Wang, R. Degraeve, B. Govoreanu, M. Jurczak, D. J. Wouters and L. Altimime, *Appl. Phys. Lett.* **97** (2010) 243509.
21. Z. T. Xu, K. J. Jin, L. Gu, Y. L. Jin, C. Ge, C. Wang, H. Z. Guo, H. B. Lu, R. Q. Zhao and G. Z. Yang, *Small* **8** (2012) 1279.
22. J. P. Shi, Y. G. Zhao, H. J. Zhang, H. F. Tian and X. P. Zhang, *Appl. Phys. Lett.* **94** (2009) 192103.
23. P. Gao, Z. Kang, W. Fu, W. Wang, X. Bai and E. Wang, *J. Am. Chem. Soc.* **132** (2010) 4197–4201.
24. M. Sirena, N. Haberkorn, M. Granada, L. B. Steren and J. Guimpel, *J. Appl. Phys.* **105** (2009) 033902.
25. P. Orgiani, C. Aruta, R. Ciancio, A. Galdi and L. Maritato, *Appl. Phys. Lett.* **95** (2009) 013510.
26. S. M. Sze, *Semiconductor Devices: Physics and Technology* (John Wiley & Sons, 2008).
27. P. Han, K. J. Jin, H. B. Lu, Q. L. Zhou, Y. L. Zhou and G. Z. Yang, *Appl. Phys. Lett.* **91** (2007) 182102.
28. S. F. Guo, *Solid State Electron.* **27** (1984) 537.
29. K. Horio and H. Yanai, *IEEE Trans. Electron Devices* **37** (1990) 1093.
30. K. Yang, J. R. East and G. I. Haddad, *IEEE Trans. Electron Devices* **41** (1994) 138.
31. P. Han, K. J. Jin, Y. Zhou, X. Wang, Z. Ma, S. F. Ren, A. G. Mal'shukov and K. A. Chao, *J. Appl. Phys.* **99** (2006) 074504.
32. K. H. Yang, J. R. East and G. I. Haddad, *Solid State Electron* **36** (1993) 321.
33. N. Biskup and A. de Andres, *Phys. Rev. B* **74** (2006) 184403.
34. S. Picozzi, C. Ma, Z. Yang, R. Bertacco, M. Cantoni, A. Cattoni, D. Petti, S. Brivio and F. Ciccacci, *Phys. Rev. B* **75** (2007) 11.
35. M. L. Wilson, J. M. Byers, P. C. Dorsey, J. S. Horwitz, D. B. Chrisey and M. S. Osofsky, *J. Appl. Phys.* **81** (1997) 4971.

36. R. Mahesh and M. Itoh, *Solid State Ionics* **108** (1998) 201.
37. S. K. Ranjan and M. S. Sundar, *Solid State Sci.* **5** (2003) 549.
38. T. Saitoh, A. E. Bocquet, T. Mizokawa, H. Namatame, A. Fujimori, M. Abbate, Y. Takeda and M. Takano, *Phys. Rev. B* **51** (1995) 13942.
39. D. Fuks, S. Dorfman, J. Felsteiner, L. Bakaleinikov, A. Gordon and E. Kotomin, *Solid State Ionics* **173** (2004) 107.
40. M. Dine El Hannani, D. Rached, M. Rabah, R. Khenata, N. Benayad, M. Hichour and A. Bouhemadou, *Mater. Sci. Semicon. Proc.* **11** (2008) 81.
41. Y. Nohara, S. Yamamoto and T. Fujiwara, *Phys. Rev. B* **79** (2009) 159110.
42. K. J. Jin, H. B. Lu, Q. L. Zhou, K. Zhao, B. L. Cheng, Z. H. Chen, Y. L. Zhou and G. Z. Yang, *Phys. Rev. B* **71** (2005).
43. C. L. Hu, P. Han, K. J. Jin, H. B. Lu and G. Z. Yang, *J. Appl. Phys.* **103** (2008) 053701.